

# An optical time delay for the double gravitational lens system FBQ 0951+2635<sup>★</sup>

P. Jakobsson<sup>1,2</sup>, J. Hjorth<sup>1</sup>, I. Burud<sup>3</sup>, G. Letawe<sup>4</sup>, C. Lidman<sup>5</sup>, and F. Courbin<sup>6</sup>

<sup>1</sup> Niels Bohr Institute, Astronomical Observatory, University of Copenhagen, Juliane Maries Vej 30,  
2100 Copenhagen Ø, Denmark  
e-mail: pallja@astro.ku.dk

<sup>2</sup> Science Institute, University of Iceland, Dunhaga 3, 107 Reykjavík, Iceland

<sup>3</sup> Space Telescope Science Institute, 3700 San Martin Drive, Baltimore, MD 21218, USA

<sup>4</sup> Institut d'Astrophysique et de Géophysique, ULg, Allée du 6 Août 17, B5C, 4000 Sart Tilman (Liège), Belgium

<sup>5</sup> European Southern Observatory, Casilla 19, Santiago, Chile

<sup>6</sup> Laboratoire d'Astrophysique, École Polytechnique Fédérale de Lausanne, Observatoire,  
1290 Chavannes-des-bois, Switzerland

Received 8 June 2004 / Accepted 13 October 2004

**Abstract.** We present optical *R*-band light curves of the double gravitationally lensed quasar FBQ 0951+2635 from observations obtained at the Nordic Optical Telescope between March 1999 and June 2001. A time delay of  $\Delta\tau = 16 \pm 2$  days ( $1\sigma$ ) is determined from the light curves. New constraints on the lensing geometry are provided by the position and ellipticity of the lensing galaxy. For a  $(\Omega_m, \Omega_\Lambda) = (0.3, 0.7)$  cosmology, the time delay yields a Hubble parameter of  $H_0 = 60_{-7}^{+9}$  (random,  $1\sigma$ )  $\pm 2$  (systematic)  $\text{km s}^{-1} \text{Mpc}^{-1}$  for a singular isothermal ellipsoid model and  $H_0 = 63_{-7}^{+9}$  (random,  $1\sigma$ )  $\pm 1$  (systematic)  $\text{km s}^{-1} \text{Mpc}^{-1}$  for a constant mass-to-light ratio model. In both models, the errors are mainly due to the time-delay uncertainties. Non-parametric models yield  $H_0 = 64_{-7}^{+9}$  (random,  $1\sigma$ )  $\pm 14$  (systematic)  $\text{km s}^{-1} \text{Mpc}^{-1}$ .

**Key words.** gravitational lensing – galaxies: quasars: individual: FBQ 0951+2635 – cosmology: cosmological parameters

## 1. Introduction

Refsdal (1964) was the first to point out the possibility of determining  $H_0$  through gravitational lensing of a variable source. Since the light travel times for the various images are unequal, intrinsic variations of the source will be observed at different times in the images. In particular, the time delay between images is a measurable parameter related to the gravitational potential of the lens and  $H_0$ . There is also a weaker dependence on cosmological parameters and on the source ( $z_s$ ) and lens ( $z_d$ ) redshifts.

Prompted by the successful optical measurements of time delays in QSO 0957+561 (Schild & Thomson 1997; Kundić et al. 1997) and PG 1115+080 (Schechter et al. 1997), we

conducted photometric monitoring campaigns of gravitationally lensed quasars at the Nordic Optical Telescope (NOT) in La Palma and at the 1.5-m Danish Telescope in La Silla between 1997 and 2001, yielding four time delays. The first one was obtained for the doubly imaged quasar B1600+434 which is lensed by an edge-on spiral (Burud et al. 2000). Then Hjorth et al. (2002) estimated the delay for the two (summed) components of RX J0911+0550. Finally, delay measurements were obtained for the doubly lensed quasars HE 2149–2745 (Burud et al. 2002a) and SBS 1520+530 (Burud et al. 2002b). These observations increased the total number of firm time-delay measurements in gravitational lenses to ten (e.g. Kochanek & Schechter 2004).

In this paper we present the fifth result from our programme: the time-delay measurement in the doubly-image quasar FBQ 0951+2635<sup>1</sup>. It was discovered by Schechter et al. (1998, hereafter S98) as a double quasar with angular separation of  $1''.1$ . The images are fairly bright with mean *R*-band magnitudes of 16.9 and 18.0 for A and B, respectively. The time delay between the two images is expected to be relatively short, of the order of one month. The monitoring

<sup>★</sup> Based on observations made with the Nordic Optical Telescope, operated on the island of La Palma jointly by Denmark, Finland, Iceland, Norway, and Sweden, in the Spanish Observatorio del Roque de los Muchachos of the Instituto de Astrofísica de Canarias. Based on observations made with ESO Telescopes at the Paranal Observatories under programme ID 66.A-0062(A). Based on observations made with the NASA/ESA Hubble Space Telescope, obtained from the Data Archive at the Space Telescope Science Institute, which is operated by the Association of Universities for Research in Astronomy, Inc., under NASA contract NAS 5-26555. These observations are associated with program #7887.

<sup>1</sup> In the literature, this lens system is also referred to as FBQS J0951+2635 or FBQS 0951+2635.

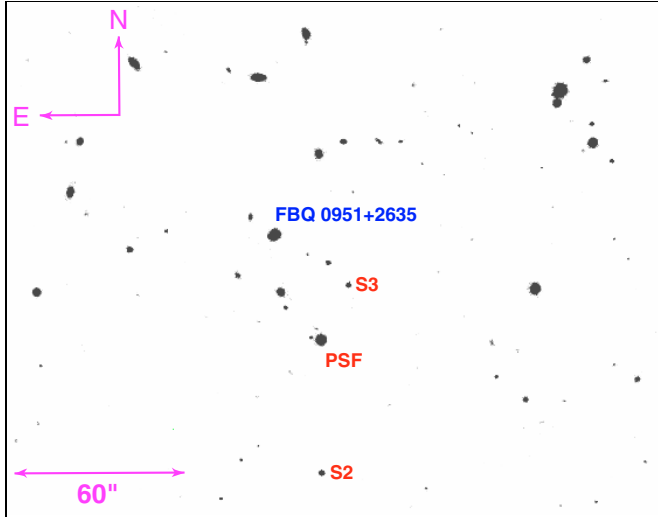


**Fig. 1.** A finding chart for FBQ 0951+2635. The star used to model the point spread function (PSF) is indicated. The two reference stars (labeled S2 and S3) used for the photometry are also marked.

programme, the light curves and the time delay are discussed in Sects. 2–4. Spectroscopic observations with the Very Large Telescope (VLT), including a measurement of the source redshift and the detection of microlensing, are reported in Sect. 5. In Sect. 6 we analyse an HST/NICMOS image to constrain a mass model of the galaxy and use it to estimate  $H_0$ . Finally, the main results are summarised in Sect. 7.

## 2. Observations and data reduction

The system was observed on a regular basis at the NOT, starting in March 1999. For the first 18 months it was observed roughly twice per month but thereafter around once per week. The target is visible from the beginning of October to the end of June, which results in gaps of about  $\sim 3$  months in the light curves. There were additional gaps due to periods of bad weather and bad seeing. Two different instruments were used: Andalucia Faint Object Spectrograph and Camera (ALFOSC) and the Standby CCD Camera (StanCam), equipped with detectors yielding pixel scales of  $0''.188$  and  $0''.176$ , respectively. In Fig. 1 the central region of the field of view of ALFOSC is displayed. One data point typically consisted of 1–3 exposures of five minutes each. The seeing varied from  $0''.7$  to  $2''.8$  during the roughly two years of observations, with  $0''.9$  being the most frequent value. All the imaging data were pre-processed (bias-subtracted and flat-field corrected) using standard IRAF routines.

## 3. Photometry

The photometric data consist of one stacked frame per epoch. Accurate photometry of the blended quasar images is crucial for time-delay measurements and all data were analysed with the versatile deconvolution algorithm developed by Magain et al. (1998, hereafter MCS). This algorithm has already been used to analyse the data of several blended quasar images (e.g. Burud et al. 2000, 2002a,b; Hjorth et al. 2002). The main

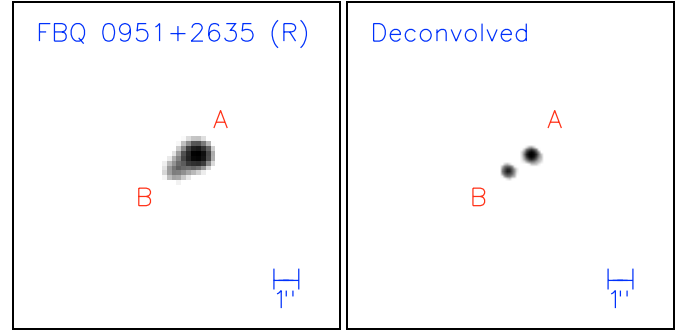


**Fig. 2.** *Left:* stacked  $R$ -band image of a  $12'' \times 12''$  region centered on FBQ 0951+2635. The seeing is  $\sim 1''.2$  and the total exposure time is  $\sim 8.3$  h. *Right:* deconvolved image ( $FWHM = 0''.28$ ) obtained from the simultaneous deconvolution of 49 frames. North is up and east to the left.

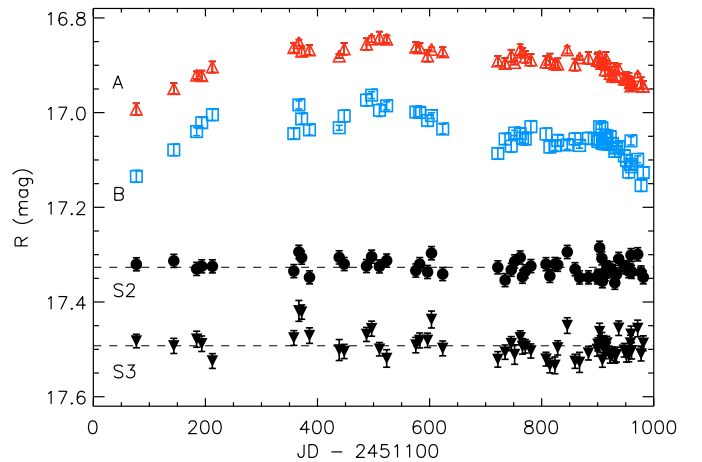


**Fig. 3.** The A and B component  $R$ -band light curves for FBQ 0951+2635 and two reference stars in the field. The plotted values are  $R - 0.9$  for B,  $R - 1.8$  for S2 and  $R - 2.0$  for S3. The magnitudes are calculated relative to the calibrated PSF star in the field. The error bars represent photon noise and PSF errors estimated from the deconvolution of the two reference stars. Since S2 and S3 are significantly fainter than components A and B, their photon noise is larger. The dashed horizontal lines represent the mean magnitudes of stars S2 and S3.

advantage of using the MCS deconvolution in the case of a photometric monitoring of a target is its ability to deconvolve all the frames from different epochs simultaneously. This constrains the positions of the two quasar images, which do not vary with time. The intensities, however, are allowed to vary from one image to the other, hence producing the light curves.

The two quasar components are clearly distinguished in our deconvolved image of FBQ 0951+2635 (see Fig. 2), but the lensing galaxy remains too faint to be detected. Although this is clearly a disadvantage when measuring the redshift of the galaxy (Sect. 5), it is fortuitous for the time-delay estimate since a contamination by an extended object could complicate the analysis.

The light curves of FBQ 0951+2635 consist of 58 data points in the  $R$ -band, as presented in Fig. 3. The magnitudes are calculated relative to the magnitude of the point spread function (PSF) star ( $R = 16.6$ ) shown in Fig. 1. Two other stars

were deconvolved as well to check for systematic errors. The error bars include both photon noise and additional systematic errors, e.g. PSF errors. The latter are estimated by using the reference stars, as explained in Burud et al. (2000).

#### 4. Time-delay estimate

It is clear from Fig. 3 that the quasar did not show large intrinsic variations. But a direct comparison of the first five data points of the two components indicates that the time delay is very short since the gradual rise in the B component closely follows the rise in the A component. In addition, during the last  $\sim 100$  days the light curves display a nearly simultaneous decrease in flux.

During the observations, a possible tiny short-lived feature was detected in both components as shown in the top panel of Fig. 4. Sliding the light curves across one another to find the best visual agreement, and making use of this feature, lead us to a rough estimate for the time delay of  $\sim 15$  days. The light curves show that A is the leading component. Once light curves of quasar components are obtained, statistical methods are needed to determine the time delay more accurately. Using the  $\chi^2$  minimization method described in Burud et al. (2001), a more objective value of  $\Delta\tau = 17 \pm 4$  days ( $1\sigma$ ) is found from the light curves. The magnitude difference between the A and B images is  $1.01 \pm 0.01$  mag, corresponding to a flux ratio between the A and B components of  $F_A/F_B = 2.54 \pm 0.02$ . The errors quoted here are obtained from Monte Carlo simulations of 1000 sets of light curves, assuming that the photometric errors are uncorrelated and follow a Gaussian distribution.

The method used to reach the aforementioned estimate adds a linear term to one of the components, thus modelling slow microlensing effects (in Sect. 5 we find independent evidence for microlensing in FBQ 0951+2635 by analysing its spectra). This linear correction does not remove all the external variations as can be seen in the middle panel of Fig. 4. Faster variations on time scales of 50–100 days are still present. The best method for dealing with such high-order variations is the iterative version of the algorithm (Burud et al. 2001). It was also applied to the light curves in an attempt to correct for these fast variations. This method yields  $\Delta\tau = 13 \pm 4$  days ( $1\sigma$ ), slightly lower than the value found with the direct method but still in agreement within the error bars.

The uncertainties remain large because our method actually finds two possible time delays for the whole data set when applying only the linear term. In addition to the 17 days, we also find that 25 days are consistent with the light curves. The result is sensitive to a smoothing parameter in the program, which smooths out dates without data points on the model curve. Since there are large gaps in our light curves, we explore various values for the parameter and find the latter result is less robust, with 17 days a more stable result. To verify this, we also ran the programme on the last 38 data points spanning a 260 day interval (shown in the top panel of Fig. 4), which do not include any large gaps and are more frequently sampled. In addition, this interval includes the potential short-lived feature. This approach yields a time delay of  $\Delta\tau = 16 \pm 2$  days ( $1\sigma$ ), with no sign of a second possible minimum. The magnitude

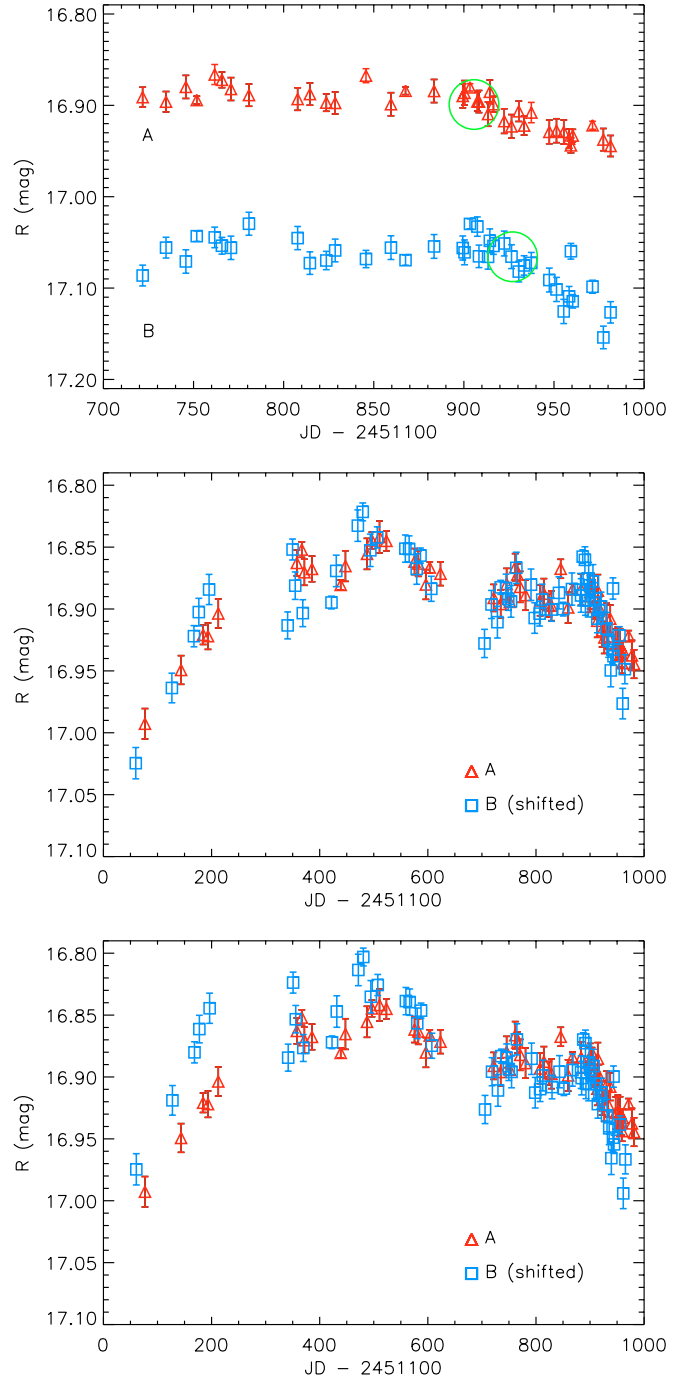


**Fig. 4.** *Top:* a zoom in on the light curves produced from the latest observations. The plotted values are  $R - 0.9$  for the B component in order to ease the comparison. A short-lived dip in the light curves is indicated by the two circles. *Middle:* time-delay shifted light curves of FBQ 0951+2635. B is shifted by +1.01 mag and forward in time by 17 days. A linear correction for the external variations is applied. *Bottom:* time-delay shifted light curves of FBQ 0951+2635. B is shifted by +1.06 mag and forward in time by 16 days. Only the last 38 data points were used with a direct method (no correction for external variations).

difference between the A and B images is  $1.06 \pm 0.01$  mag, corresponding to  $F_A/F_B = 2.65 \pm 0.02$ . The resulting shifted light curves are displayed in the bottom panel of Fig. 4. In the same figure there are signs of possible microlensing variations

**Table 1.** Estimated time delays and  $R$ -band magnitude differences for FBQ 0951+2635 calculated with three different methods. The quoted uncertainties are  $1\sigma$  errors.

Method	$\Delta\tau$ (days)	$\Delta m$ (mag)
$\chi^2$ fit	$17 \pm 4$	$1.01 \pm 0.01$
Iterative fit	$13 \pm 4$	–
Last 38 points	$16 \pm 2$	$1.06 \pm 0.01$

in one of the components for the first few hundred days. This microlensing is most likely the result of compact objects in the lensing galaxy (positioned close to the B component; see below), located in the line-of-sight towards the quasar images. This result is further strengthened by the independent spectroscopic microlensing observations in Sect. 5.

The time-delay estimates and magnitude offsets obtained from our three different approaches are consistent with each other and are presented in Table 1. Given that the large gaps in our light curves affect our results, we adopt  $\Delta\tau = 16 \pm 2$  days as the best estimate for the time delay.

## 5. VLT spectroscopy

The redshift of the lensing galaxy has proved elusive. S98 found absorption lines attributed to Mg II at  $z = 0.73$  and  $z = 0.89$  in both spectra of the quasar components. From the position of the lens on the fundamental plane, Kochanek et al. (2000) suggested  $z_d = 0.21$  with a range of 0.18–0.23, while Kochanek et al. (1998, hereafter K98) quote a redshift of 0.24, estimated from the properties of the lensing galaxy (C. Kochanek 2002, private communication). Multiply lensed quasars have also become an important tool to detect microlensing by compact objects within the lensing galaxy. This offers the opportunity to study the spatial structure of the lensed quasar with very high angular resolution.

On 2001 March 24–25 we obtained deep optical spectra of FBQ 0951+2635 with the VLT using the Multi Object Spectroscopy (MOS) capability of FORS1 with  $1''.4$  wide slitlets. Two grisms were used, G300V+GG435 covering approximately 4300–8600 Å and G300I+GG435 with a wavelength coverage of roughly 6600–11 000 Å.

We acquired  $2 \times 1200 + 620$  s spectra with G300V and  $3 \times 1200$  s spectra with G300I. The slitlets were oriented with a position angle of  $-55^\circ.6$  to cover both quasar components and the lensing galaxy. One of the slitlets was centred on a star in the field of view whose PSF was later used as an input for deconvolution of the quasar spectra. The individual spectra were combined, yielding a seeing of  $0''.4$  ( $0''.6$ ) and a spectral resolution of  $10 \text{ \AA}$  ( $16 \text{ \AA}$ )  $FWHM$  for G300I (G300V). The projected pixel size was  $0''.1 \times 2.59 \text{ \AA}$  ( $0''.1 \times 2.69 \text{ \AA}$ ) for G300I (G300V).

Redshift estimations of lensing galaxies are often limited by observational difficulties arising from the fact that the light from these galaxies can be heavily blended with the light from one of the quasar images, the latter sometimes being several magnitudes brighter. The spectral deconvolution algorithm developed by Courbin et al. (2000) is able to deconvolve

spectra in the spatial direction. It can therefore be used to separate the quasar and galaxy spectra. This technique was applied to FBQ 0951+2635 in order to deblend the spectra of the two quasar images and to search for the lensing galaxy, located only  $0''.2$  away from component B.

In the spectra of both quasar components we identify three emission lines at  $>5\sigma$ , namely C III]  $\lambda 1909$ , Mg II  $\lambda 2798$  and [O II]  $\lambda 3727$ . These lines place the quasar at  $z_s = 1.246 \pm 0.001$ , a value fully consistent with that found by White et al. (2000). In addition, the absorption lines first reported by S98, interpreted as the Mg II doublet at  $z = 0.729$  and  $z = 0.892$ , are detected in the A component. In the spectrum of the B component we only detect the  $z = 0.892$  system.

Strong equivalent width (EW) difference exists between the Mg II line in the spectra of the two quasar images, with EW a factor of 1.46 smaller in component B than in component A with high significance. The most probable explanation is that the continuum emission of the B component is microlensed by compact objects in the lensing galaxy. This result is consistent with standard models of quasar structure, with the scale of the broad emission line region significantly greater than that of the continuum source (e.g. Wambsganss et al. 1990; Krolik 1999). The Mg II flux ratio between A and B is  $3.7 \pm 0.3$ . This is considerably higher than the continuum flux ratio ( $\sim 2.5$ ) and that from broadband photometry.

In order to obtain the lensing galaxy spectrum, free of any contamination by the two bright nearby quasar images, the 2-D spectrum of FBQ 0951+2635 was spatially deconvolved. However, the signal-to-noise ratio was very low in the lensing galaxy spectrum. Due to this and a lack of significant absorption and emission lines in the spectrum, we were unable to determine a spectroscopic redshift. In what follows we adopt  $z_d = 0.24$  from K98, but note that decreasing  $z_d$  from 0.26 to 0.18 decreases the value of  $H_0$  by 37%.

## 6. Lens modelling

The time delay and redshifts measured for FBQ 0951+2635 can be used to infer an estimate of  $H_0$ , based on modelling of the total gravitational potential responsible for the lensing effect. This includes the main lensing galaxy and any tidal perturbations from objects near it or along the line of sight. FBQ 0951+2635 is not an easy case to model, as the lensing galaxy is not readily visible. However, as seen in the left panel of Fig. 5, there is a small “lightbump” northwest of, but close to the B component.

We use two distinct approaches to convert the time delay into  $H_0$ : parametric models that involve an analytical form for the lensing galaxy, and non-parametric models that involve more degrees of freedom, i.e. a pixelated surface density (Saha & Williams 1997; Williams & Saha 2000; Saha & Williams 2004).

### 6.1. HST/NICMOS results

In March 1998, four 640 s images of the FBQ 0951+2635 lens system were obtained by K98, taken with the Near Infrared Camera and Multi-Object Spectrometer’s (NICMOS)

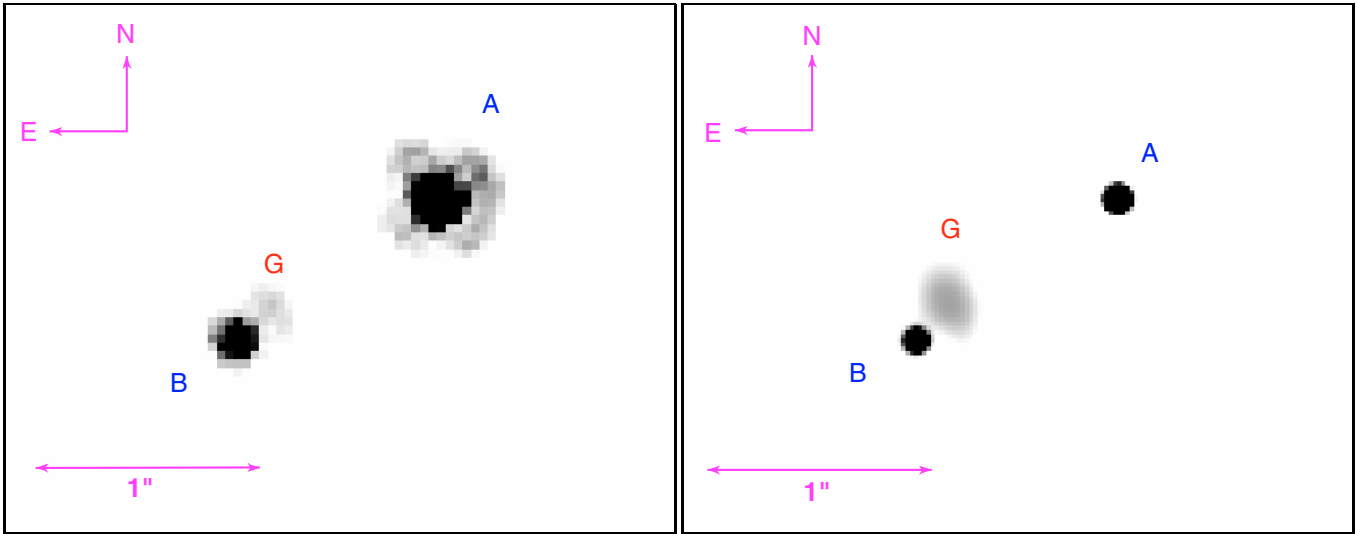


**Fig. 5.** *Left:* an HST/NICMOS image of FBQ 0951+2635. *Right:* a deconvolved HST/NICMOS image shown on a logarithmic intensity scale. In both panels the lensing galaxy is denoted by the letter “G”.

**Table 2.** Image and lens positions.

Object	$\theta_x$	$\theta_y$
Lens	$0'.000 \pm 0'.002$	$0'.000 \pm 0'.002$
A	$0'.750 \pm 0'.001$	$0'.459 \pm 0'.001$
B	$-0'.142 \pm 0'.001$	$-0'.169 \pm 0'.001$

NIC2 camera onboard the HST. The filter used was F160W. The images were drizzled to give a pixel scale of  $0'.0375$ .

We deconvolved the drizzled image, using the A component as an empirical PSF. The right panel of Fig. 5 shows the result from the deconvolution: the lensing galaxy is positioned close to the B component. This lens configuration is in full agreement with the fact that A is the leading component (see Sect. 4), as predicted by gravitational lens theory. We fit ellipses to the isophotes in the core of the lensing galaxy resulting in an ellipticity of  $e = 0.25 \pm 0.04$  and a position angle (PA) of  $22^\circ \pm 4^\circ$ . Assuming that the mass distribution follows the light distribution we can restrict ourselves to these ranges of ellipticities and PAs. For the de Vaucouleurs model (see below) we also estimated the effective radius, resulting in  $R_e = 0'.09 \pm 0'.02$ . The exact positions of the quasar images are listed in Table 2 in a lens-centered coordinate system. The quasar images have an angular separation of  $1'.091 \pm 0'.001$ , while the B component is positioned  $0'.221 \pm 0'.002$  from the center of the lensing galaxy. We note that our position of the galaxy obtained from the HST/NICMOS image is quite different from that published by S98, where a lens candidate is detected midway between the two components. But the S98 data were ground-based and they acknowledge that the candidate might be a spurious detection.

## 6.2. Analytical models

Using the *lensmodel* package (Keeton 2001), we fit the lens system with a dark matter model and a constant  $M/L$  model.

The former is a singular isothermal ellipsoid (SIE) model with a flat rotation curve, while the latter is the prototypical constant  $M/L$  model: the de Vaucouleurs model. This is a similar approach as Kochanek & Schechter (2004) carried out for four lens systems with known time delays measured by Burud et al. (2000, 2002a,b) and Schechter et al. (1997). The SIE model sets a lower bound on  $H_0$ , while the constant  $M/L$  model sets an upper bound on  $H_0$ . This results from the fact that no galaxy in a cold dark matter dominated Universe should have mass distributions which are more centrally concentrated than the luminosity distribution (Mo et al. 1998). In addition, a typical lensing galaxy should not have a rising rotation curve at approximately twice the effective radius, making the SIE the least concentrated reasonable model.

During the fit, the astrometry of the quasar images relative to the lens is fixed, as well as the redshift of the source and lens. The models are constrained by using the range of ellipticities and PAs obtained in Sect. 6.1. In addition, we use  $F_A/F_B$  as a constraint. Four values have been derived independently. In Sect. 4 we found from broadband photometry that  $F_A/F_B = 2.5\text{--}2.7$ . This is similar to the ratio calculated from the spectral continua (Sect. 5). On the other hand, the emission line flux ratio is measured to be  $F_A/F_B = 3.7 \pm 0.3$  (Sect. 5). Finally, S98 report the radio emission line ratio to be  $4.7 \pm 0.6$ . While flux ratios from broadband photometry are generally known to be unreliable due to the ever present possibility of microlensing, the emission line fluxes should reflect the “true” flux ratio (e.g. Wisotzki et al. 2003). Hence, in what follows, we adopt  $F_A/F_B = 3.7 \pm 0.3$  as a model constraint, but note that allowing  $F_A/F_B$  to vary between 2.5 and 4.7 does change the value of  $H_0$  by only approximately 4%.

The free parameters in our model include the mass of the lensing galaxy, the source coordinates and flux, and the amplitude of the external shear ( $\gamma$ ) along with the direction to it. We include shear in our models since at least two mass concentrations lie along the line of sight, namely the ones responsible for the Mg II absorption systems (S98; Sect. 5).

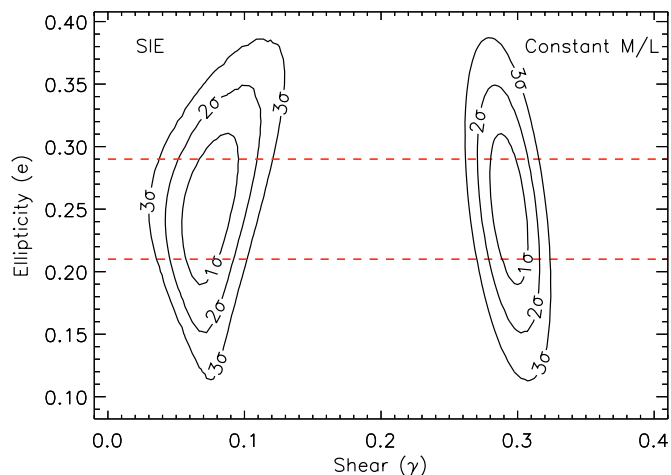


**Fig. 6.**  $\Delta\chi^2$  contours for FBQ 0951+2635 in the plane of the ellipticity ( $e$ ) and shear ( $\gamma$ ). The contours are drawn at  $\Delta\chi^2 = 2.30, 6.17$  and  $11.8$ , corresponding to the  $1\sigma, 2\sigma$  and  $3\sigma$  confidence intervals for two degrees of freedom. There is a weak degeneracy between  $e$  and  $\gamma$ . The area between the horizontal dashed lines is the range of the measured ellipticity.

It is important to understand any degeneracies between the two sources of angular structure in the model, the ellipticity and shear. The external shear breaks the circular symmetry of the lens and therefore it has the same effect as introducing ellipticity in the lens. Figure 6 shows the contours of the  $\Delta\chi^2$  in the space of  $e$  and  $\gamma$  after optimizing all other parameters. In the SIE model this results in a moderate shear of  $\gamma = 0.07$ , while for the constant  $M/L$  model there is a large shear of  $\gamma = 0.29$ . By evaluating  $H_0$  inside the  $1\sigma$  contours in Fig. 6 we get an estimate for the systematic uncertainties in both models. If we take the currently most popular cosmology, i.e.  $\Omega_m = 0.3$ ,  $\Omega_\Lambda = 0.7$ , and  $\Delta\tau = 16$  days, we find  $H_0 = 60_{-7}^{+9}$  (random,  $1\sigma$ )  $\pm 2$  (systematic)  $\text{km s}^{-1} \text{Mpc}^{-1}$  for the SIE model, while  $H_0 = 63_{-7}^{+9}$  (random,  $1\sigma$ )  $\pm 1$  (systematic)  $\text{km s}^{-1} \text{Mpc}^{-1}$  for the constant  $M/L$  model. Due to the relatively low redshift of the lensing galaxy, the influence of a change in cosmology is small compared to the measurement errors. Adopting other cosmologies,  $(\Omega_m, \Omega_\Lambda) = (1.0, 0.0)$  or  $(\Omega_m, \Omega_\Lambda) = (0.3, 0.0)$ , will change the inferred value of  $H_0$  by only about 4% for this lens system.

### 6.3. Pixelated models

While the mass distribution of the pixelated models of Saha & Williams (2004) is not as well related to the physical parameters of the lens, the models allow an exploration of a wide range of lens shapes. Thus, this approach better constrains the systematic errors as it is unrestricted by the confines of the parametric models.

We fit the lens system with the *Pixelens* programme<sup>2</sup>. During the fit, the ellipticity of the mass distribution was kept free. As in the analytical models, we added external shear. The lensing galaxy appears unperturbed in Fig. 5, leading us to

<sup>2</sup> <http://ankh-morpork.maths.qmw.ac.uk/~saha/astron/lens/pix/>

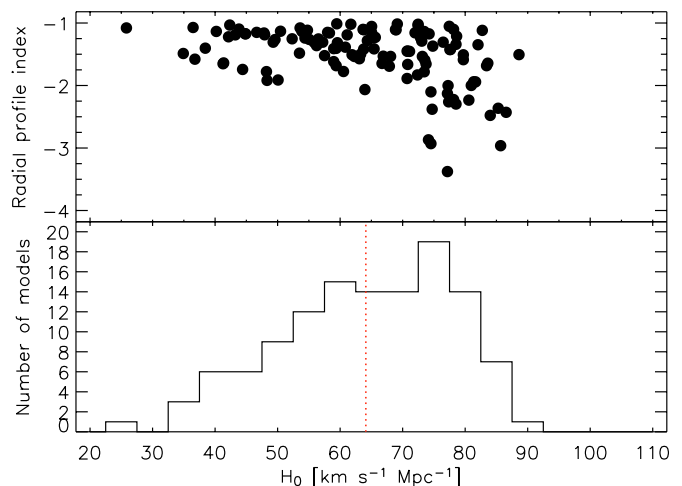


**Fig. 7.** *Top:* the slope of the projected mass density profile plotted against  $H_0$  for 121 different non-parametric models. *Bottom:* probability distribution of the derived  $H_0$  values for the same models as above. The median value of the distribution is indicated by the dotted line.

enforce the inversion symmetry constraint (i.e. the lens looks the same if rotated by  $180^\circ$ ). In order to avoid models less concentrated than the SIE, we imposed a constraint stating that the index of the projected radial mass density profile ( $\alpha$ ) must be steeper than  $-1$ . As there is not an option in *Pixelens* to invoke this constraint, we ran a total of 500 models and, in the upper panel of Fig. 7, plot those 121 that fulfill  $\alpha < -1$ . Most lens systems, when modelled independently, show a correlation between  $\alpha$  and  $H_0$ , in the sense that steeper density profiles result in higher values of  $H_0$ . FBQ 0951+2635 shows this correlation rather weakly. The lower panel of Fig. 7 displays the derived  $H_0$  probability distribution. The mean of the distribution is calculated to be  $H_0 = 64_{-7}^{+9}$  (random,  $1\sigma$ )  $\pm 14$  (systematic)  $\text{km s}^{-1} \text{Mpc}^{-1}$ .

## 7. Discussion

The time delay  $\Delta\tau = 16 \pm 2$  days ( $1\sigma$ ) has been measured in the lensed quasar FBQ 0951+2635 on the basis of  $R$ -band images obtained with the NOT. Due to the lack of pronounced features in the light curves and because the time delay is short compared to the sampling of the light curves,  $\Delta\tau$  is not very well constrained, thus explaining the large error bars. If this short time delay is to be pinned down more accurately, intensive monitoring should be performed in the future. As long as the variability is sufficiently strong and erratic during the observations, this should help constrain  $\Delta\tau$  even further.

Applying an SIE lens model to the case of FBQ 0951+2635, we derive  $H_0 = 60_{-7}^{+9}$  (random,  $1\sigma$ )  $\pm 2$  (systematic)  $\text{km s}^{-1} \text{Mpc}^{-1}$ , where the error bars incorporate the uncertainty in the measured time delay as well as the uncertainties in the lens model due to the degeneracy between the shear and ellipticity. For a constant  $M/L$  model we estimate  $H_0 = 63_{-7}^{+9}$  (random,  $1\sigma$ )  $\pm 1$  (systematic)  $\text{km s}^{-1} \text{Mpc}^{-1}$ . These two analytical models were studied because they represent the limiting case for physically possible mass

distributions given our current understanding of dark matter. Non-parametric models employed on the lens system resulted in  $H_0 = 64^{+9}_{-7}$  (random,  $1\sigma$ )  $\pm 14$  (systematic)  $\text{km s}^{-1} \text{Mpc}^{-1}$ , with a relatively broad range in  $\alpha$ .

Unfortunately we cannot determine which mass profile is appropriate given the available data. However, by using an independent  $H_0$  estimate we can try to break the degeneracy. The local estimate by the HST Key Project (Freedman et al. 2001) is  $H_0 = 72 \pm 8 \text{ km s}^{-1} \text{Mpc}^{-1}$ , the recent results by WMAP (Spergel et al. 2003) indicate that  $H_0 = 71^{+4}_{-3} \text{ km s}^{-1} \text{Mpc}^{-1}$ , while the value of  $H_0 = 59 \pm 6 \text{ km s}^{-1} \text{Mpc}^{-1}$  by Saha et al. (2001) is based on Cepheid calibration for a sample of galaxies with Type Ia supernovae. Due to our large  $\Delta\tau$  uncertainty, all three estimates are consistent with the models we adopt. It is therefore important to monitor this lens system more frequently in order to beat down the random uncertainty on any  $H_0$  estimate from FBQ 0951+2635.

*Acknowledgements.* It is a pleasure to thank Chuck Keeton for helpful discussions about lens modelling. We thank the anonymous referee for his/her critical reading and useful comments on the paper. We are especially grateful to Anlaug Amanda Kaas and the many visiting observers at NOT who have contributed to this project by performing the scheduled observations. We thank Gunnlaugur Björnsson and Einar Gudmundsson for constructive comments and suggestions. P.J. gratefully acknowledges support from a special grant from the Icelandic Research Council. F.C. acknowledges financial support from the European Commission through Marie Curie grant MCFI-2001-0242 and the Pôle d'Attraction Interuniversitaire, P5/36 (PPS Science Policy, Belgium). Some of the optical data presented here have been taken using ALFOSC, which is owned by the Instituto de Astrofísica de Andalucía (IAA) and operated at the Nordic Optical Telescope under agreement between IAA and the NBIfAFG of the Astronomical Observatory of Copenhagen. This work was supported by the Danish Natural Science Research Council (SNF).

## References

- Burud, I., Hjorth, J., Jaunsen, A. O., et al. 2000, *ApJ*, 544, 117  
 Burud, I., Magain, P., Sohy, S., & Hjorth, J. 2001, *A&A*, 380, 805  
 Burud, I., Courbin, F., Magain, P., et al. 2002a, *A&A*, 383, 71  
 Burud, I., Hjorth, J., Courbin, F., et al. 2002b, *A&A*, 391, 481  
 Courbin, F., Magain, P., Kirkove, M., & Sohy, S. 2000, *ApJ*, 529, 1136  
 Freedman, W. L., Madore, B. F., Gibson, B. K., et al. 2001, *ApJ*, 553, 47  
 Hjorth, J., Burud, I., Jaunsen, A. O., et al. 2002, *ApJ*, 572, L11  
 Keeton, C. R. 2001, *ApJ*, submitted [arXiv:astro-ph/0102340]  
 Krolik, J. H. 1999, *Active Galactic Nuclei: From the Central Black Hole to the Galactic Environment* (Princeton: Princeton University Press)  
 Kochanek, C. S., & Schechter, P. L. 2004, *The Hubble Constant from Gravitational Lens Time Delays*, in *Measuring and Modeling the Universe*, ed. W. L. Freedman (Cambridge: Cambridge University Press), 117  
 Kochanek, C. S., Falco, E. E., Impey, C. D., et al. 1998, *CASTLeS*, <http://cfa-www.harvard.edu/glensdata> (K98)  
 Kochanek, C. S., Falco, E. E., Impey, C. D., et al. 2000, *ApJ*, 543, 131  
 Kundić, T., Turner, E. L., Colley, W. N., et al. 1997, *ApJ*, 482, 75  
 Magain, P., Courbin, F., & Sohy, S. 1998, *ApJ*, 494, 472 (MCS)  
 Mo, H. J., Mao, S., & White, S. D. M. 1998, *MNRAS*, 295, 319  
 Refsdal, S. 1964, *MNRAS*, 128, 307  
 Saha, P., & Williams, L. 1997, *MNRAS*, 292, 148  
 Saha, P., & Williams, L. 2004, *AJ*, 127, 2604  
 Saha, A., Sandage, A., Tammann, G. A., et al. 2001, *ApJ*, 562, 314  
 Schechter, P. L., Bailyn, C. D., Barr, R., et al. 1997, *ApJ*, 475, L85  
 Schechter, P. L., Gregg, M. D., Becker, R. H., Helfand, D. J., & White, R. L. 1998, *AJ*, 115, 1371 (S98)  
 Schild, R. E., & Thomson, D. J. 1997, *AJ*, 113, 130  
 Spergel, D. N., Verde, L., Peiris, H. V., et al. 2003, *ApJS*, 148, 175  
 Wambsganss, J., Paczyński, B., & Schneider, P. 1990, *ApJ*, 358, L33  
 White, R. L., Becker, R. H., Gregg, M. D., et al. 2000, *ApJS*, 126, 133  
 Williams, L., & Saha, P. 2000, *AJ*, 119, 439  
 Wisotzki, L., Becker, T., Christensen, L., et al. 2003, *A&A*, 408, 455